# COHERENCE DECOMPOSITION ANALYSIS, A CASE STUDY IN THREE GORGES AREA, CHINA

**T. Wang[1,2], M. Liao[1], D. Perissin[2] and F. Rocca[2]**

*(1) Wuhan University, P.O. Box C310, 129# Luoyu Road, 430079 Wuhan, China, Email: wangteng@lmars.whu.edu.cn*

*(2) Politecnico di Milano, Via Giuseppe Ponzio, 34/5, 20133 Milan, Italy*

## ABSTRACT

SAR interferometric coherence losses are due to different decorrelation sources. In this paper, we decompose the coherence sources into surface and point-like components. Using the geometry relationship between two acquisitions and SRTM DEM, one can get the value of the geometrical coherence loss, which is the main part of surface coherence loss. After removing the coherence losses due to geometry and azimuth, temporal coherence can be obtained. Besides temporal coherence, point-like targets can be identified from the coherence decomposition analysis, in given spatial and temporal baseline conditions. The results are validated with optical images and Permanent Scatterers analyses.

## 1. INTRODUCTION

InSAR coherence is very useful in many applications, such as image classification, target detection, etc [1-4]. For different targets, coherence indicates their geometry and physical characters. For example, water body always show near to zero coherence due to the changing surface and low backscattering coefficient; distributed targets such as agricultural fields show a moderate coherence after one day and low coherence after one months; rocks and buildings in cities show high coherence even after years. The relation between coherence and targets' physical extension in certain normal baseline and frequency difference conditions is also described in [5].

It is well known that the coherence map of an interferogram contains not only temporal change information between two acquisitions, but also geometrical and azimuthal coherence losses [6]. In mountainous areas, because of steep terrain, different local slopes also affect the geometry coherence. The wavenumber shift principle describes this phenomenon very well [7]. From this theory, range filtering can be used to remove the non-overlapping parts of the two images' spectra. However, if there is a point-like target in a resolution cell, range filtering will destroy the coherent information because the point-like target is not affected by geometry de-correlation. In other words, if in a tandem data set with very limited temporal de-correlation we remove systematically the estimated azimuthal and geometrical coherence losses from a coherence estimate window (CEW) with a point-like target, the coherence there will be greater than 1. This gives us a clue to identify point-like scatterers from just one interferogram.

From the coherence estimation point of view, there are some areas with unusually distributed scatterers in the CEWs, for example, in foreshortening areas. As the local slope nearly equals the incidence angle of SAR, the geometrical coherence is close to 0, i.e. no surface coherence information can be derived there. It's easy to flag out such areas by considering the standard deviation (std) of the real value of the complex signal in a CEW. If the std crosses a given threshold, we will call it a unusually distributed CEW. However, we face the risk that a point-like target may also make the std of real in a CEW larger than that threshold. In this situation, the solution here is that for unusually distributed CEWs, we only decompose those with meaningful coherence, i.e. larger than 0.5. The others are flagged out as 0.

In summary, the purpose of this paper is to decompose the coherence into different components as below:

1) surface coherence;
   a) geometry coherence;
   b) azimuth coherence;
   c) temporal coherence.
2) point-like targets coherence
   a) point-like targets coherence in unusually distributed CEW;
   b) point-like targets coherence in usually distributed CEW.

Firstly, the std of real part of the complex value in every CEW is calculated and the unusual CEWs are flagged. Then, take advantage of geometry relationship between two acquisitions and azimuth and range bandwidth of the SAR system, the value of geometrical and azimuthal coherence components are estimated. An algorithm to get the local slope in SAR slant range coordinate from Shuttle Radar Topographic Mission (SRTM) DEM is also carried out in this step. After removing the two components of the coherence as mentioned above, temporal coherence can be obtained to indicate the physical changes between acquisition times in the illustrated terrain. Besides surface coherence, the possible point-like targets are identified as well with their coherence. Finally, we validate our results in test

site Badong, Three Gorges area, China, with optical image and spatial coherence map from Permanent Scatterers (PS) analysis.

## 2. COHERENCE ESTIMATION

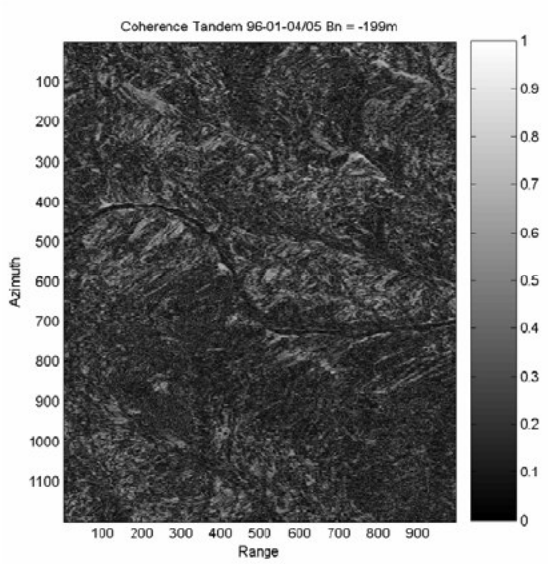


(a)

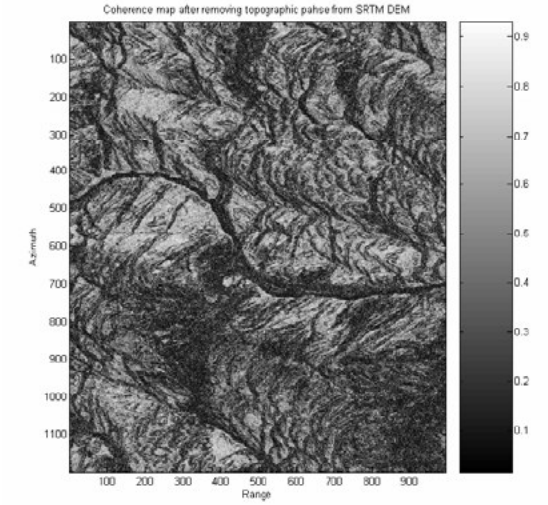


(b)

*Figure 1 coherence map of the test site. (a) with topographic phase; (b) after removal of the topographic phase.*

The coherence can be estimated over a moving window by comparing the radar returns as in Eq. 1 [8]. For SAR interferometry, the argument of $\hat{\gamma}$ is the averaged interferogram phase. Generally speaking, the phases in a CEW change progressively in both azimuth and range directions, and this can be estimated from the interferogram itself [9]. However, in mountainous areas as our test site, the topographic phase strongly affects the coherence estimation. Here, the SRTM DEM is used to remove the topographic phase before estimating the coherence. The algorithm used here to get the height of every pixel from SRTM DEM is described in [10]. The difference between the coherence map before and after removing topographic phase in our test site is shown in Fig. 1 (a) and (b).

$$\hat{\gamma} = \frac{\sum_{i=1}^{L} S_{1i} S_{2i}^{*} \cdot e^{j\phi(i)}}{\sqrt{\sum_{i=1}^{L} |S_{1i}|^2} \sqrt{\sum_{i=1}^{L} |S_{2i}|^2}} \qquad (1)$$

Anther problem for coherence decomposition in mountainous areas is that, in the foreshortening areas, the local slope is near the SAR incidence angle, the ground resolution cell becomes very large, and the wavenumber shift is unlimited. In these areas, no coherence exists between two acquisitions. Because when the coherence magnitude is very low, i.e. lower than 0.2, the sampled estimator we use will be biased to higher values [8], there it will be difficult to get correct targets information by removing geometrical coherence. We flagged such areas by comparing the std of the real value within the CEW. When the std is more than 2 times of the real value std of the whole image, we flag the coherence of this CEW as 0 for decomposition analyses.

## 3. ESTIMATION OF THE GEOMETRICAL AND AZIMUTHAL COHERENCE COMPONENTS

The estimation of azimuthal coherence loss is made easy from the Doppler central frequency recorded in the header file of SLC images. The ratio between the Doppler frequency shift and the azimuth bandwidth is calculated to get the azimuth coherence of several pixels.

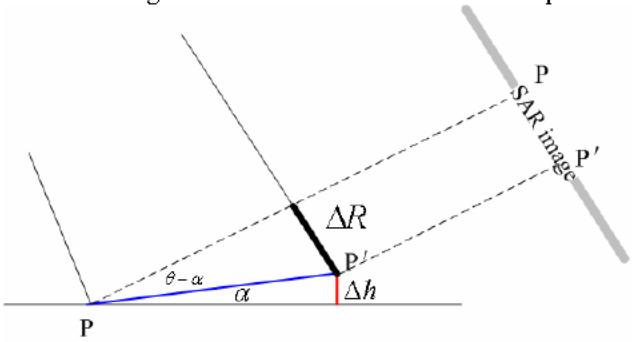


*Figure 2 local slope geometry*

For geometry coherence, the wavenumber shift between master and slave images can be described as Eq. 2 [5]. Here, $c$ is the velocity of light, $\lambda$ is the wavelength, $B_{\perp}$ is the normal baseline, $r_1$ is the slant range between sensor and resolution cell on the ground, $\theta$ is the incidence angle and $\alpha$ is the local slope. The parameters

in Eq. 2 can be obtained from SAR geometry except the local slope $\alpha$ .

$$\Delta f = -\frac{c}{\lambda}\frac{B_{\perp}}{r_1(\theta-\alpha)} \qquad (2)$$

Since every pixel's height has been obtained from the SRTM DEM during the coherence estimation, the height difference of adjoined pixels $\Delta h$ is known. Then from Fig. 2, the geometry relationship between the local slope $\alpha$ and ground resolution $Res_G$ can be indicated and described in Eq. 3 and Eq. 4..

$$Reg_G = \frac{c}{2B_r \sin(\theta-\alpha)} \qquad (3)$$

$$\frac{\Delta h}{Res_G} = \sin\alpha \qquad (4)$$

After simple mathematics, $\alpha$ can be estimated from known image parameters as well as range bandwidth $B_r$, $\theta$ and $\Delta h$ as in Eq. 5. Then, the geometrical coherence component for every pixel can be got from the ratio between wavenumber shift $\Delta f$ and $B_r$. Fig. 3 and Fig. 4 show the estimated azimuthal and geometrical coherence components in our test site.

$$\tan\alpha = \frac{\sin\theta}{\frac{c}{2\Delta h B_r} + \cos\theta} \qquad (5)$$

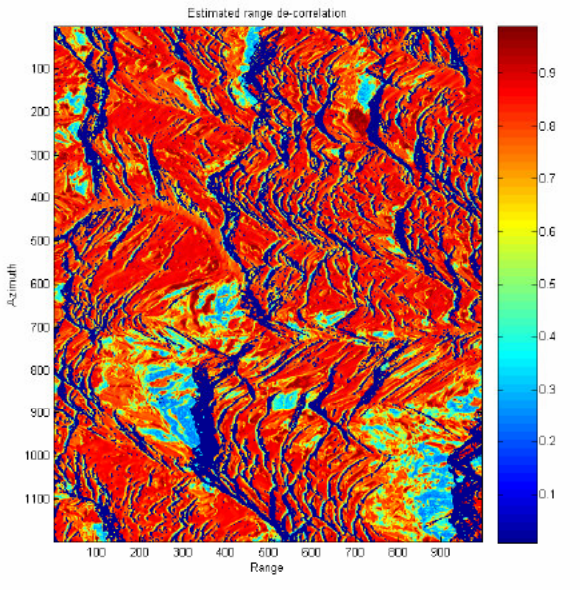


*Figure 3 estimated geometrical coherence component*

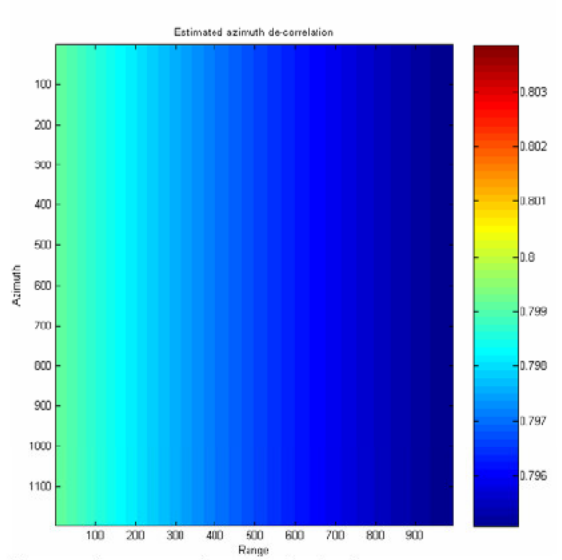


*Figure 4 estimated azimuthal coherence component*

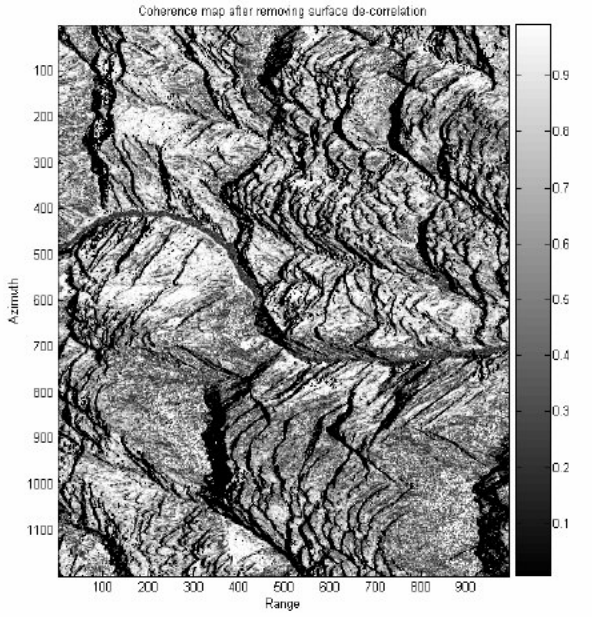


*Figure 5 estimated temporal coherence*

## 4. COHERENCE DECOMPOSITION

If we ignore the decorrelation due to thermal noise and processing, the surface coherence of distributed targets are composed of azimuth, geometry and temporal coherence [6]:

$$\left|\gamma_{\text{surface}}\right| = \left|\gamma_{\text{azimuth}}\right| \cdot \left|\gamma_{\text{geometry}}\right| \cdot \left|\gamma_{\text{temporal}}\right| \qquad (7)$$

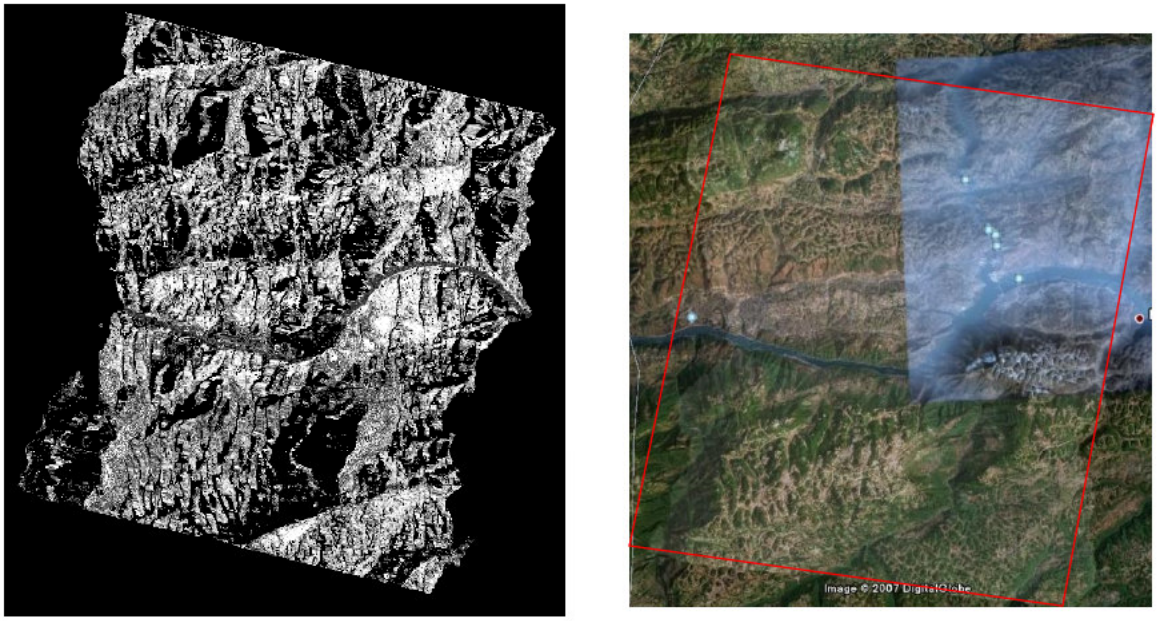


*Figure 6 Geocoded temporal coherence map with optical image form Google Earth*

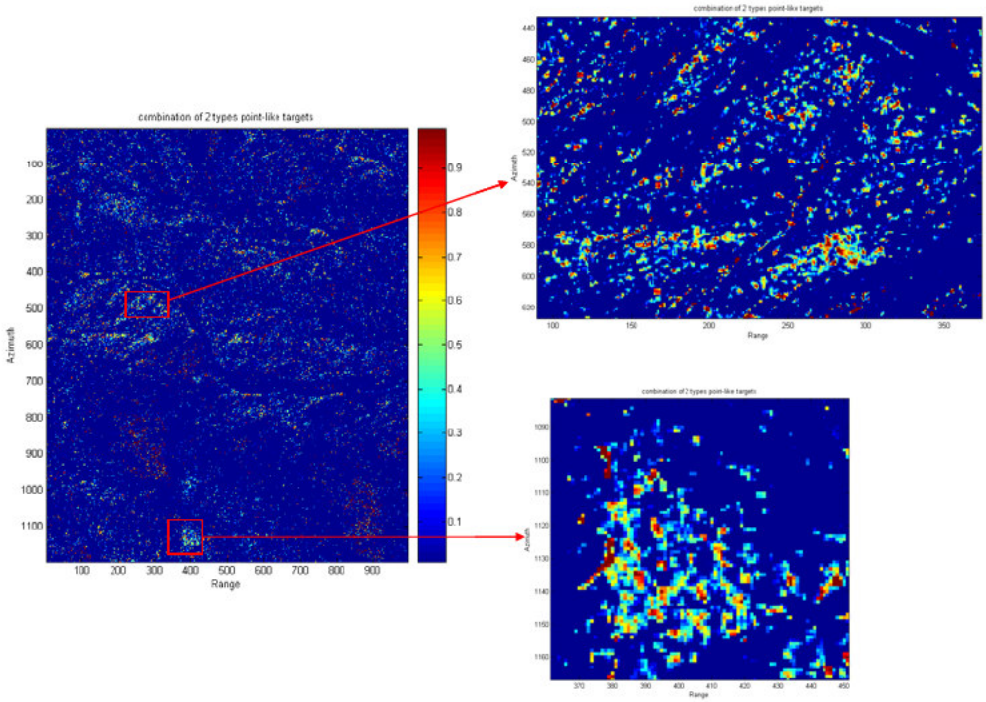


*Figure 7 possible point-like targets in the spatial and temporal baseline conditions of the test site (199m, one day).*

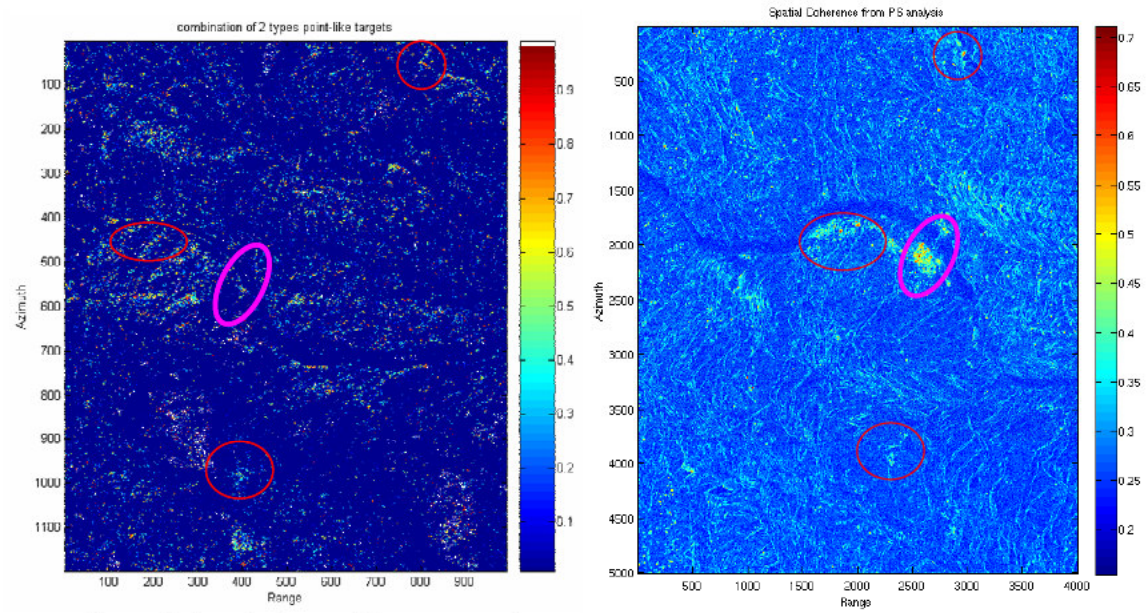


*Figure 8 identified point-like targets with spatial coherence from PS analysis. The red circles indicate the same distribution of point-like targets and the purple circle indicates the new Badong city, which was not built in our data acquiring time*

For point-like scatterers, since they do not suffer from the surface decorrelation, it's easy to identify them because their coherence will be larger than 1 after removing the estimated surface coherence. The data set used here is a pair of ERS-1/2 tandem data in January, 1996 to minimize the affection of temporal decorrelation. The normal baseline is 199m. The test site locates in Badong, Three Gorges area, China. This area is famous for its steep terrain and surface changes after the Three Gorges Dam is built in 2003. The CEW used here is 15 in azimuth and 3 in range. And the coherence map is averaged with the factor of five in azimuth.

### 4.1. Surface coherence

Fig. 5 shows the estimated temporal coherence after removing the azimuthal and geometrical coherence components from the sampled estimated coherence map. Any unusually distributed CEW is flagged as 0, so the foreshortening areas can be distinguished from other low coherence areas such as water bodies, shadows etc.

Comparing with Fig. 1 (b), the vegetation distribution, which shows moderate coherence, can be identified more clearly. Furthermore, the extent of vegetation flourish can be indicated without the influence of ever changing local slopes. This improvement can be used for a correct interpretation of the coherence map. Also, if we compare the right bottom corner of Fig. 1 (b) and Fig. 5, the vegetation distribution can be distinguished from low geometry coherence and foreshortening area.

Using Google Earth images of this area, we see that the geocoded temporal coherence map is strongly related to the physical characters of the ground scatterers, which are shown in Fig. 6. Along the Yangtze River, the riverside in the west part shows low coherence due to flourishing vegetation; the east part riverside shows almost complete coherence due to the Badong city and bare rocks. In other areas, the same phenomena can be found. For future work, if the optical image of the same acquiring time with InSAR coherence map can be collected, more reasonable validation will be presented.

### 4.2. Point-like targets coherence

As discussed in section 1, the coherence of the CEW within a point-like target will be greater than 1 after removing the geometrical and azimuthal coherence components. This kind of point-like targets can be identified from coherence decomposition analysis. In unusually distributed CEWs, another type of point-like scatterers appears by considering the original coherence map. Different from foreshortening areas, the point-like targets, which make the std of real in the CEWs be greater than the threshold show very high coherence. If we set certain threshold for example 0.5, it's easy to select out them from unusually distributed CEWs.

When both types of point-like targets are identified, their coherence values are linearly scaled to 0-1. The possible point-like targets in the spatial and temporal baseline conditions of our test site (199m, one day) are shown in Fig. 7. From the zoom in vision of the

scatterers, it's clear that the point scatter did not only affect one CEW, where it is located but also their adjoining CEWs. This is because the coherence is estimated in moving CEWs. The CEW with point-like scatterer in the centre has the highest coherence, in the surrounding CEWs, reduced coherence values are observed.

Fig. 8 shows the cross validation with the spatial coherence map derived from PS analysis. The PS processing combined more than 30 scenes of ERS and ENVISAT data of this area from 1993 to 2006. Because the short spatial and temporal baseline, the number of possible point-like scatterers from coherence decomposition are obviously more than the high spatial coherence pixels from PS analysis. Most of the possible PSs are identified from coherence decomposition analysis as we indicated in red circle.

However, many points within the purple circle, which includes the highest temporal average coherence in PS Analysis, did not appear in our point-like scatterers coherence map. That's because the new city of Badong was built after 1997 to host the migration when the Three Gorges Dam was going to be constructed. Our data set is acquired in 1996, when there were in that area not as many artificial targets.

## 5. CONCLUSIONS

In this paper, a new idea to analyze the coherence is presented. Instead of filtering, we remove the geometrical and azimuthal correlation losses by estimating them from sensor parameters and SRTM DEM. The benefits of our method are in three main aspects: 1), the point-like coherence information, which will be destroyed by filtering is reserved; 2) all the processing are performed within a CEW (here, 15 in azimuth and 3 in range), smaller than the usual filter stencil; 3) the estimation of geometry and azimuth coherence is much faster.

The processing of surface coherence decomposition can be seen as a kind of image stretching. The information we need (such as temporal coherence) is enhanced by removing the information we don't need here (such as azimuth and geometry coherence). For point-like targets, our method offers an effective way to identify them from only one interferogram. Our future work will focus on the information extraction from the point-like targets.

## 6. ACKNOWLEDGEMENT

The works in this paper are funded by National Key Basic Research and Development Program of China (No. 2007CB714405) and 863 High Technology Program of China (Contract No. 2006AA12Z123). The authors would like to thank ESA for providing the SAR data through ESA-NRSCC Dragon Cooperation Programme (id2567) as well as the whole Tele-Rilevamento Europa staff for processing the images.

## 7. REFERENCES

1. C. L. Werner, S. H., and P. Rosen (1996). Application of the interferometric correlation coefficient for measurement of surface change. In *Proc AGU Fall Meeting*, San Francisco, CA.
2. Askne, J. I. H., P. B. G. Dammert, et al. (1997). C-band repeat-pass interferometric SAR observations of the forest. *Geoscience and Remote Sensing, IEEE Transactions on* **35**(1): 25-35.
3. Santoro, M., J. I. H. Askne, et al. (2007). Observations, Modeling, and Applications of ERS-ENVISAT Coherence Over Land Surfaces. *Geoscience and Remote Sensing, IEEE Transactions on* **45**(8): 2600-2611.
4. Rosen, P. A., S. Hensley, et al. (2000). Synthetic aperture radar interferometry. *Proceedings of the IEEE* **88**(3): 333-382.
5. Perissin, D., C. Prati, et al. (2006). Validating the SAR Wavenumber Shift Principle With the ERS Envisat PS Coherent Combination. *Geoscience and Remote Sensing, IEEE Transactions on* **44**(9): 2343-2351.
6. Zebker, H. A. and J. Villasenor (1992). Decorrelation in interferometric radar echoes. *Geoscience and Remote Sensing, IEEE Transactions on* **30**(5): 950-959.
7. Gatelli, F., A. M. Guamieri, et al. (1994). The wavenumber shift in SAR inferometry. *Geoscience and Remote Sensing, IEEE Transactions on* **32**(4): 855-865.
8. Touzi, R., A. Lopes, et al. (1999). Coherence estimation for SAR imagery. *Geoscience and Remote Sensing, IEEE Transactions on* **37**(1): 135-149.
9. Zebker, H. A. and K. Chen (2005). Accurate estimation of correlation in InSAR observations. *Geoscience and Remote Sensing Letters, IEEE* **2**(2): 124-127.
10. Liao, M., T. Wang, et al. (2007). Reconstruction of DEMs from ERS-1/2 Tandem Data in Mountainous Area Facilitated by SRTM Data. *Geoscience and Remote Sensing, IEEE Transactions on* **45**(7): 2325-2335.